Electronic Supplementary Material (ESI) for Nanoscale Horizons.

Unveiling the Formation Mechanism of the Biphenylene Network

Kaifeng Niu[1,2], Qitang Fan[3], Lifeng Chi[2,4*], Johanna Rosen[1], J. Michael Gottfried[3*], Jonas Björk[1*]

[1]*Department of Physics, Chemistry and Biology, IFM, Linköping University, 581 83 Linköping, Sweden*
[2]*Institute of Functional Nano & Soft Materials (FUNSOM) and Jiangsu Key Laboratory for Carbon-Based Functional Materials & Devices, Soochow University, Suzhou 215123, China*
[3]*Department of Chemistry, Philipps-Universität Marburg, 35032 Marburg, Germany*
[4] *Department of Materials Science and Engineering, Macau University of Science and Technology, Macau 999078, China*

Corresponding Authors

*Lifeng Chi: chilf@suda.edu.cn

* J. Michael Gottfried: michael.gottfried@chemie.uni-marburg.de

*Jonas Björk: jonas.bjork@liu.se

Contents

Methods

DFT calculations

All density functional theory calculations were performed by Vienna ab-initio simulation package (VASP) together with atomic simulation environment (ASE).[1,2] The electron-ion interactions were described by the projector augmented wave (PAW) potentials,[3] together with a plane wave basis expanded to a kinetic energy cutoff of 400 eV. The van der Waals density functional (vdW-DF) in the version of rev-vdWDF2 was employed to treat the exchange-correlation interactions.[4,5] Such method has shown to accurately describe the adsorption of molecules on metal surfaces.[6,7] The Au(111) surface was by a four layered slab using a *p*(10×8) supercell and periodic image interactions were avoided by employing a 15 Å vacuum layer. The gamma point was used to sample the 1st Brillouin zone, and convergence tests were performed to the numerical accuracy of the results (see Section 8 below). The transition states were found by using a combination of the Climbing Image Nudged Elastic Band method (CI-NEB) and the Dimer method.[8,9] Firstly, 20 images were inserted between the initial and final state of each reaction step and optimized with the CI-NEB. Secondly, the central image was employed as the input of the Dimer method to obtain the saddle point. All structures including local minima and saddle points, except the bottom two layers of the Au(111) surface which were kept frozen, were optimized until the residual force on all atoms were smaller than 0.02 eV/Å. The STM images were simulated by the Tersoff-Hamman approximation with the implementation by Lorente and Persson.[10,11] In the reaction, the dissociated F and H atoms were assumed to drift far on the surface. The chemical potential of the dissociated F was defined as

$$\mu_{\mathrm{F}} = E[\mathrm{F@Au(111)}] - E[\mathrm{Au(111)}] \quad \text{(S1)}$$

in which $E[\mathrm{F@Au(111)}]$ and $E[\mathrm{Au(111)}]$ represent the potential energy of F atom adsorbed on the Au(111) and the pristine Au(111) surface. In addition, dissociated F and H pairs were treated as the HF molecule, in which the chemical potential of HF molecule was calculated by

$$\mu_{\mathrm{HF}} = E_{\mathrm{HF}}(g) \quad \text{(S2)}$$

All the chemical potentials were calculated with the 8 × 8 × 1 *k*-point sampling to achieve the numerical convergence.

The relative energy for each intermediate state is defined as

$$\Delta E_{\mathrm{Sx}} = E_{Sx} - E_{\mathrm{S0}} + F_{\mathrm{alignment}} \quad \text{(S3)}$$

in which the E_{Sx} refers to the potential energy of intermediate state with dissociated F and H atoms excluded from the system, and E_{S0} is the potential energy of the initial state (**S0**). The alignment factor $F_{\mathrm{alignment}}$ is defined as

$$F_{\mathrm{alignment}} = n \times \mu_{\mathrm{HF}} + m \times \mu_{\mathrm{F}} \quad \text{(S4)}$$

in which *n* is the number of the generated HF molecule with respect to the initial state, *m* is either 1 (for each defluorination step) or 0 (for the other reaction steps).

STM measurements

The experiments were performed under ultra-high vacuum conditions (base pressure 1×10^{-10} mbar) with an integrated variable-temperature STM and photoelectron spectrometer system (SPECS). Au(111) single crystals purchased from MaTeck were used as substrates for the growth of poly(2,5-difluoro-*para*-phenylene) chains. Preparation of clean and well-defined Au(111) surfaces was achieved by cycles of Ar^+ ion bombardment and annealing at 850 K. The 4,4''-dibromo-2,2',2'',5,5',5''-hexafluoro-1,1':4',1''-terphenyl (DHTP) precursor was vapor-deposited (evaporator temperature 400 K) onto the clean Au(111) surface held at room temperature. After deposition, the sample was post-annealed to the indicated temperatures for typically 10 min.

Entropy contribution of generated HF molecules.

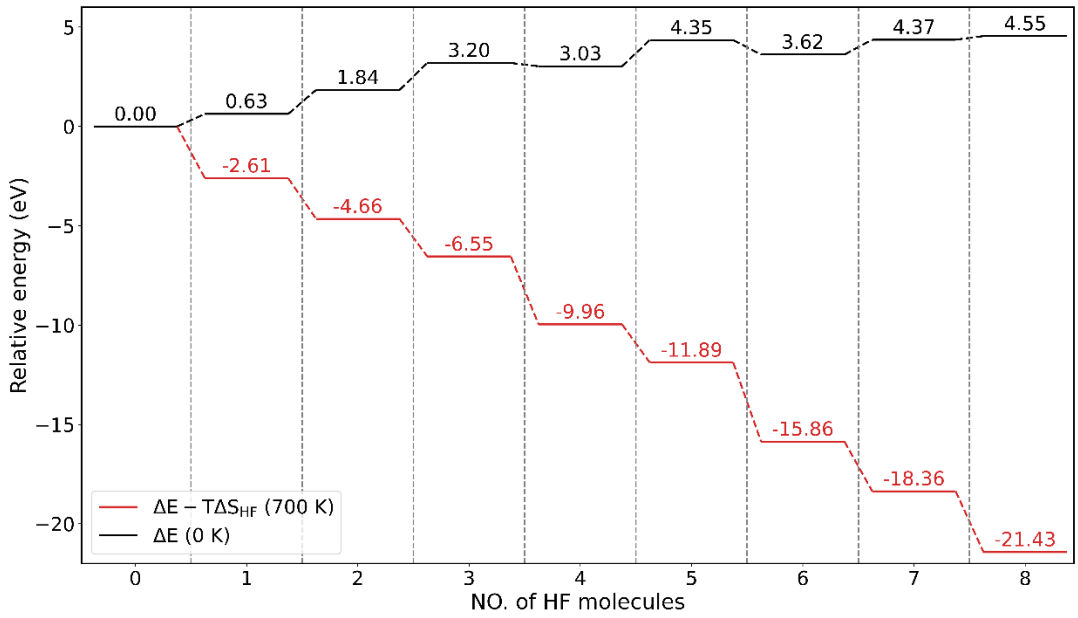

Figure S1. The stepwise energy profile of interchain HF zipping at 0 K (black curve) and 700 K (red curve).

Taking into account that the intermolecular HF zipping reactions on the Au(111) were achieved in ultrahigh vacuum and high temperature,[12] we estimated relative energies under such conditions by considering the entropy gain due to the HF elimination, which is calculated as

$$\Delta E_n(T) = E_n + n \times [E_{\mathrm{HF}}(g) - TS_{\mathrm{HF}}(T,p)] - E_0 \quad \text{(S5)}$$

where T is 700 K and p is 10^{-10} mbar based on experimental conditions. The $S_{HF}(T,p)$ is the entropy of HF at temperature T and pressure p, which is defined as[13]

$$S_{\mathrm{HF}}(T,p) = S_{\mathrm{HF}}(T,p_0) - k_{\mathrm{B}} ln(\frac{p}{p_0}) \quad \text{(S6)}$$

in which k_{B} is the Boltzmann's constant and $S_{\mathrm{HF}}(T,p_0)$ is from the tabulated value at p_0 = 1 bar.[14] As seen, the relative energies for each step decrease significantly under the experimental conditions, leading to strong exergonic characteristics. Despite that the $\Delta E_n(T)$ does not contain the vibrational enthalpy of molecules, such drastic decrease in reaction energy due to entropy of HF still indicates that the HF-zipping reactions can be thermodynamically favored at T = 700 K.

Evaluation of reaction energies

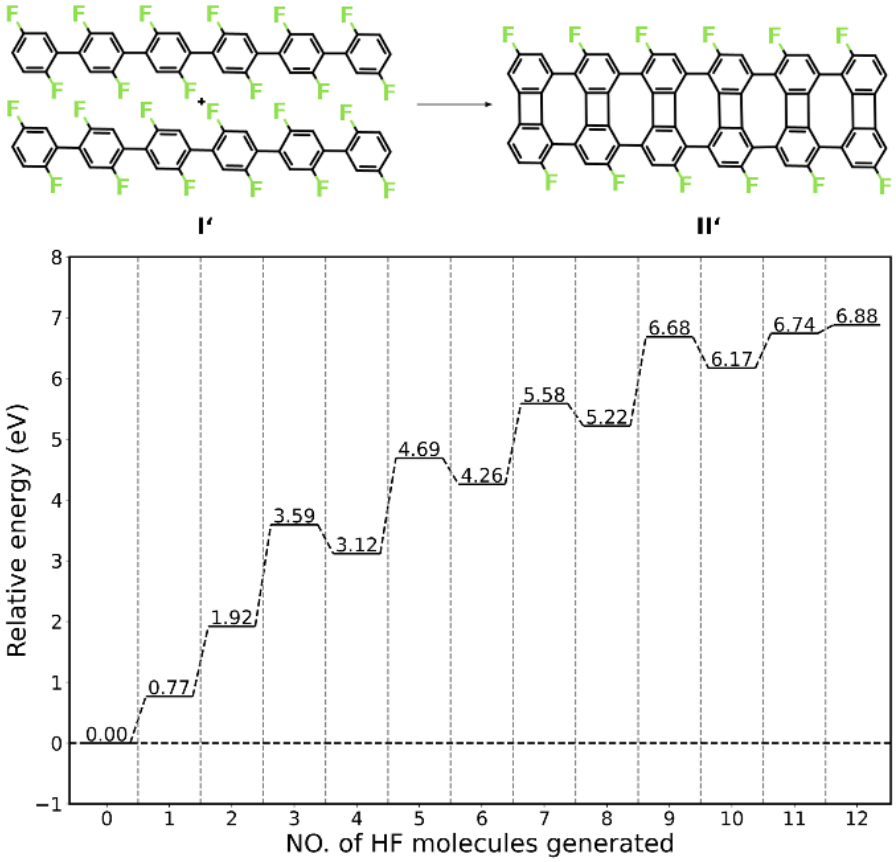

Figure S2. The stepwise energy profile for the precursor containing six difluorophenylene groups (**I'**), leading to the synthesis of the final product **II'**.

The concerted HF formation and C-C coupling

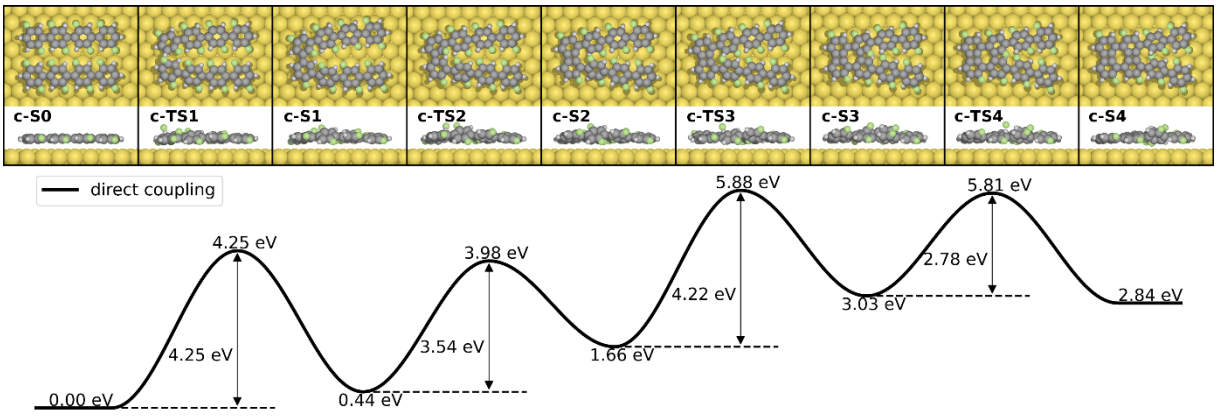

Figure S3. Reaction pathway and energy profile of the concerted HF formation and C-C coupling mechanism. Note that the such reaction pathway and energy profile are calculated on the Au(111) surface containing 3 atomic layers. Definition of energies are given in **Eq. S3** (see section 1). The C, H, F, and Au atoms are represented by the gray, white, green, and yellow spheres, respectively.

Figure S3 depicts the reaction pathway that the HF elimination and the C-C coupling take place simultaneously. However, high energy barriers indicate such pathway is energetically unfavored.

Defluorination vs. dehydrogenation

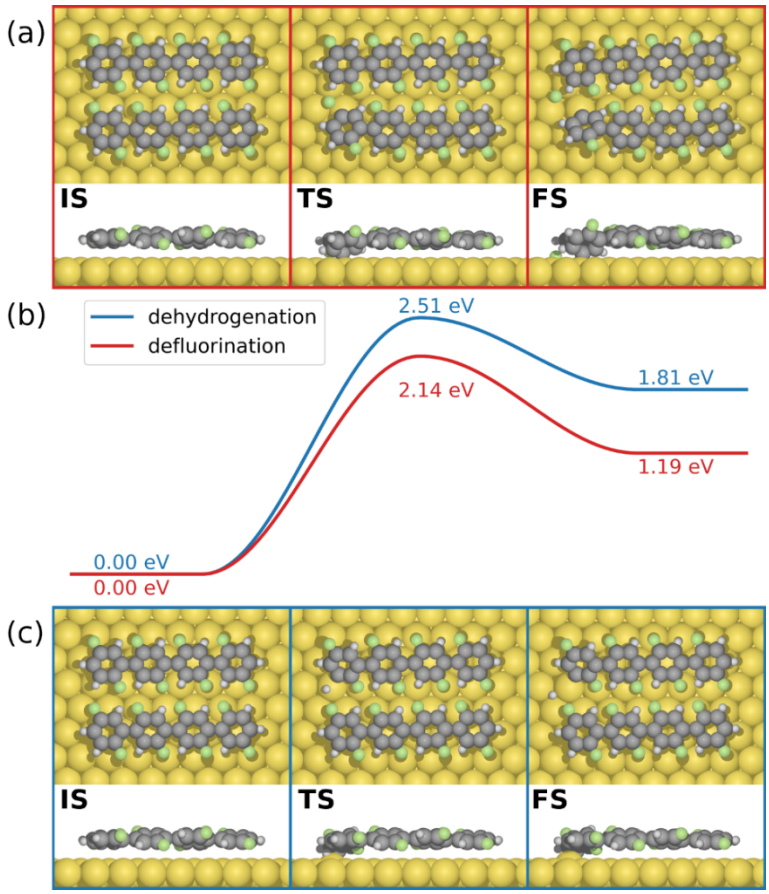

Figure S4. Reaction pathways of the (a) defluorination and the (c) dehydrogenation. (b) is the corresponding energy profile. The C, H, F, and Au atoms are represented by the gray, white, green, and yellow spheres, respectively.

Both defluorination and dehydrogenation follow the similar pathway, in which the surface Au atom serves as the active site and form the C-Au bond in the final state. Nevertheless, the defluorination exhibits lower activation energy than that of the dehydrogenation. The defluorination is therefore considered as the first step of the HF zipping.

The inter-polymer mechanism – the formation of the 1st four-membered ring

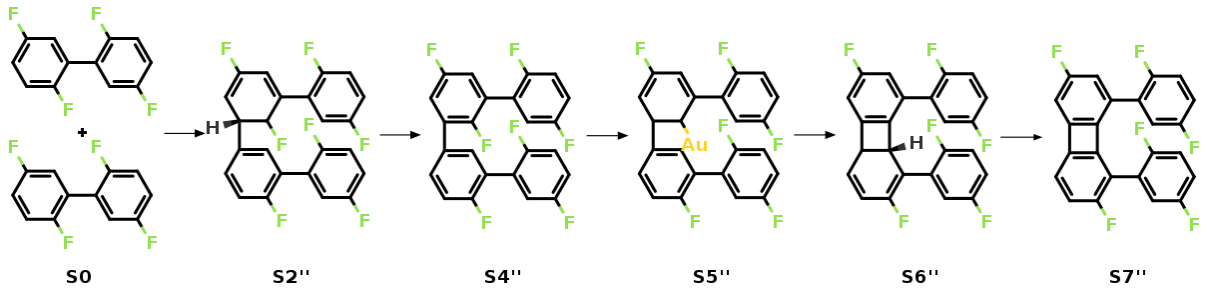

Figure S5. Interpolymer mechanism of the formation of the 1st 4 membered carbon ring. Valence structures are labeled in accordance with the calculated reaction pathway.

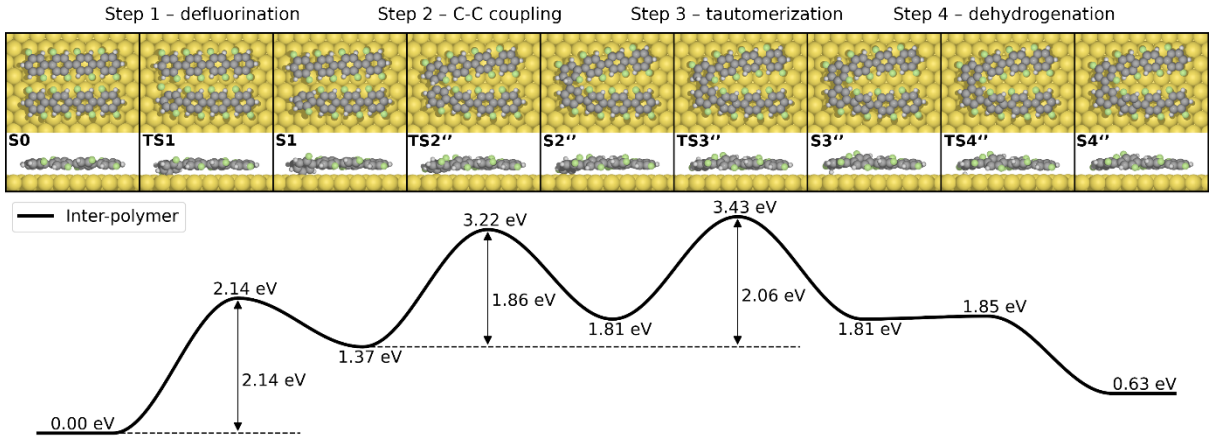

Figure S6. The reaction pathway and energy profile of 1st C-C formation with the interpolymer mechanism (species **S1** to **S3**). The pathway can be excluded by the high energy barrier of the C-C coupling (Step 2). Definition of energies are given in **Eq. S3**. The C, H, F, and Au atoms are represented by the gray, white, green, and yellow spheres, respectively.

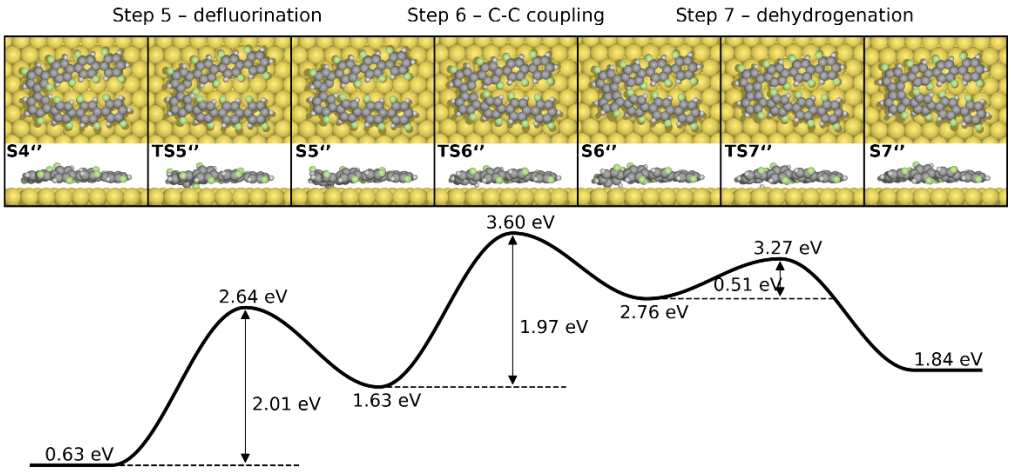

Figure S7. The reaction pathway and energy profile of the 2nd C-C formation (species **S3** to **S5**). Definition of energies are given in **Eq. S3**. The C, H, F, and Au atoms are represented by the gray, white, green, and yellow spheres, respectively.

The selectivity of the HF zipping – the four-membered ring vs. the six-membered ring

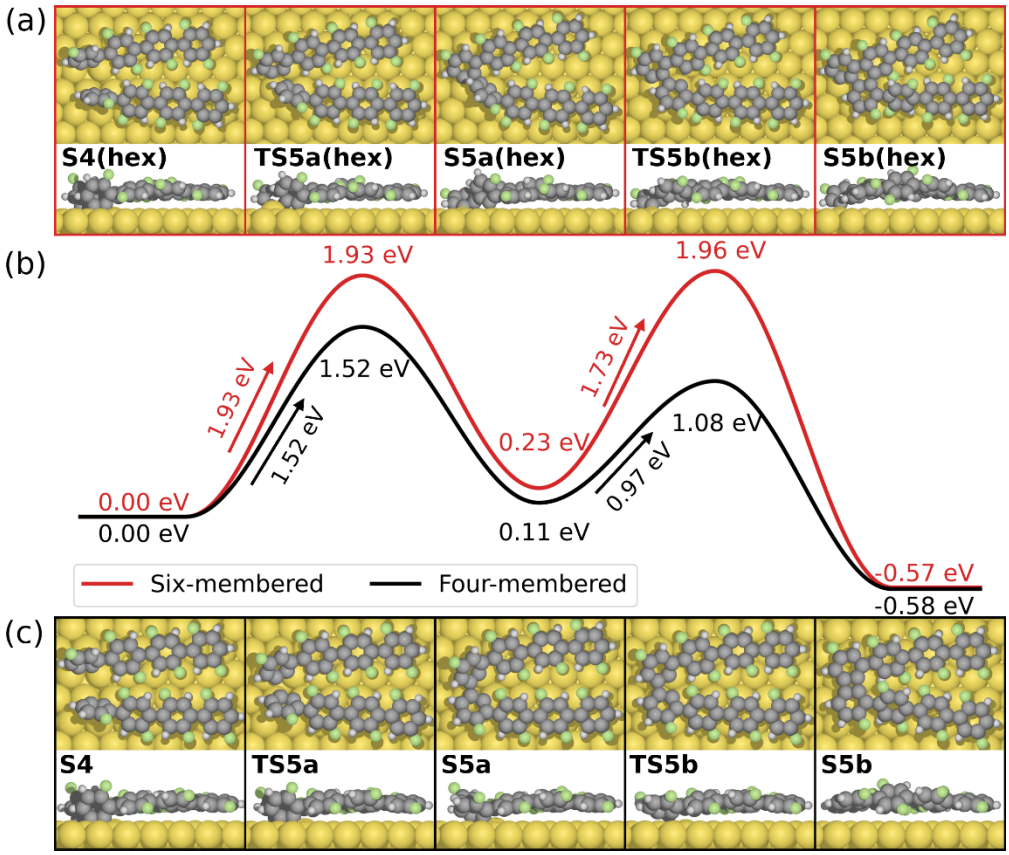

Figure S8. The reaction pathways for the formation of (a) a six-membered ring (labeled in red) and (c) a four-membered ring (labeled in black) starting from two chemisorbed phenylene group on the Au(111), with (b) corresponding energy profiles.

Figure S8 shows the reaction pathways for the formation of six- and four-membered rings. Starting from two dehydrofluorinated phenylene radicals (**S4b**), two steps are required to form the six- or four-membered ring. As seen, the formation of six-membered rings exhibits higher energy barriers at both steps (1.93 eV vs. 1.52 eV, and 1.73 eV vs. 0.97 eV). Such difference of activation energies indicate that the formation of four-membered ring is more favored than that of six-membered rings. Consequently, the BPN can be synthesized with high selectivity while the formation of graphene is suppressed.

The inter-polymer mechanism – the formation of the 2nd four-membered ring

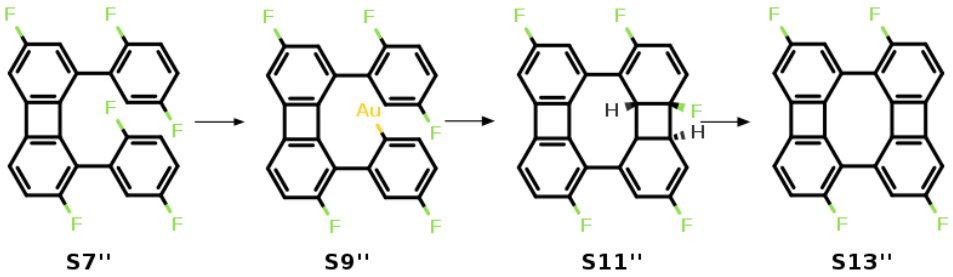

Figure S9. Interpolymer mechanism of the formation of the 2nd four-membered carbon ring. Valence structures are labeled the same way as for the calculated reaction pathway.

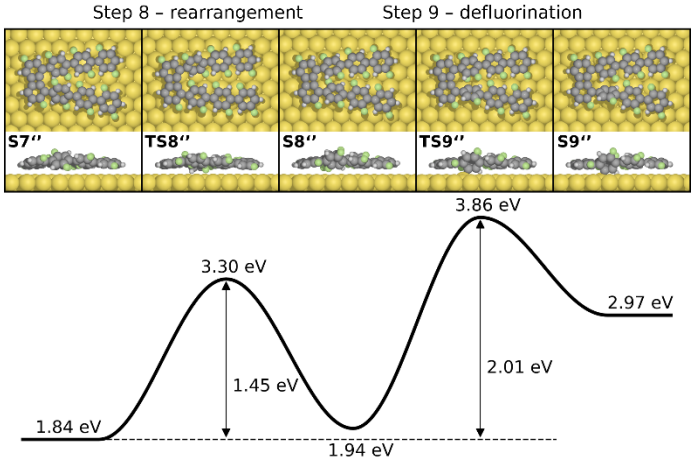

Figure S10. The reaction pathway and energy profile of the 3rd defluorination (species **S5** to **S6**). Definition of energies are given in **Eq. S3**. The C, H, F, and Au atoms are represented by the gray, white, green, and yellow spheres, respectively.

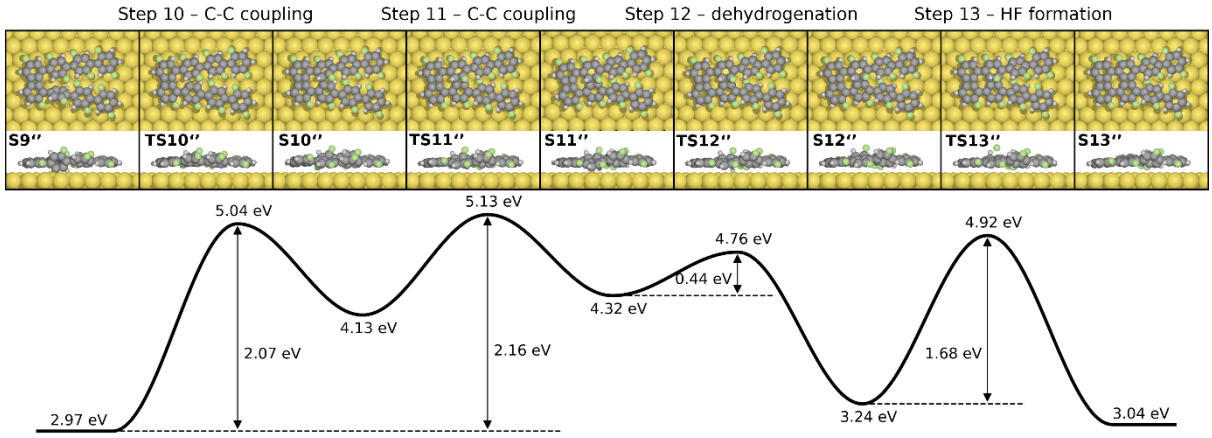

Figure S11. The reaction pathway and energy profile of the formation of the 3rd and 4th C-C bonds between two molecular chains with the interpolymer mechanism (species **S6** to **S8**). Definition of energies are given in **Eq. S3**. The C, H, F, and Au atoms are represented by the gray, white, green, and yellow spheres, respectively.

The alternative pathway for closing the 2nd four-membered ring

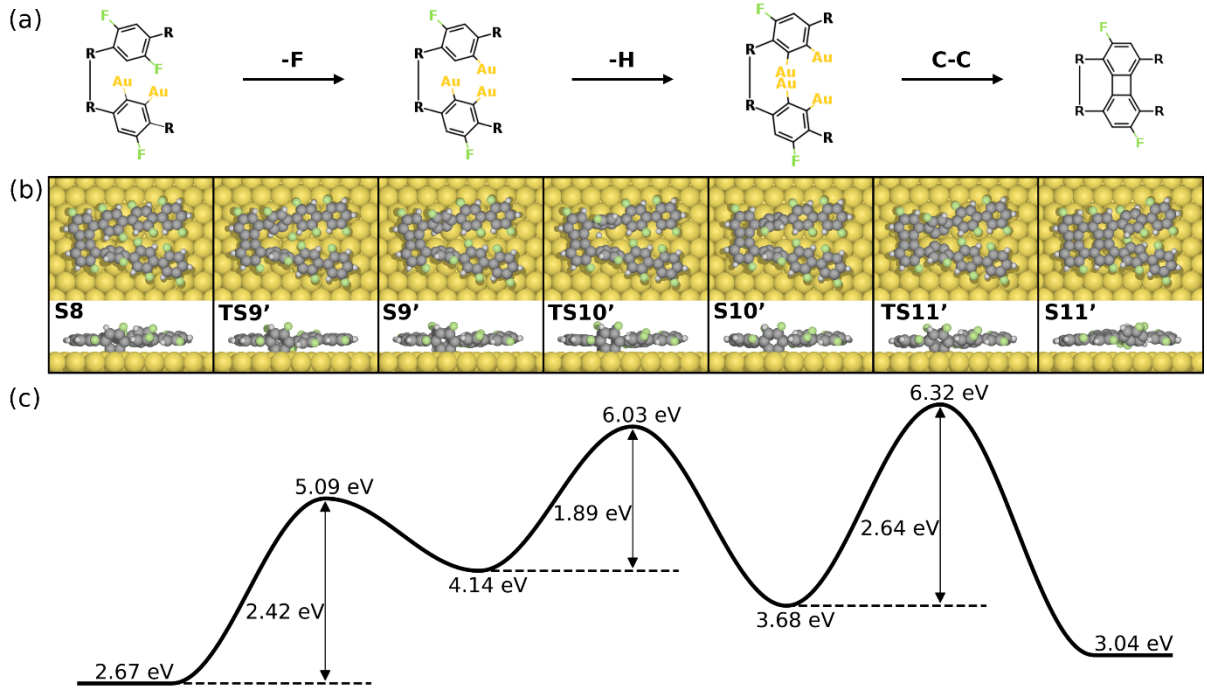

Figure S12. The alternative pathway for the formation of the 2nd four-membered ring. The reaction initiates at **S8** in **Figure 6**. The defluorination and dehydrogenation (**S8**-**S9'** and **S9'**-**S10'**) take place at the other precursor molecule. Definition of energies are given in **Eq. S3**. The C, H, F, and Au atoms are represented by the gray, white, green, and yellow spheres, respectively.

Figure S12 shows the reaction pathway for the formation of the 2nd four-membered ring following the same mechanism as that of the 1st. However, the defluorination at the other molecular precursor suffers from high activation energy caused by the mismatch between the molecule and the surface. Similar scenario can be found for the subsequent dehydrogenation and the C-C coupling step. Both reactions exhibit higher energy barrier owing to the strong steric hindrance.

K points sampling convergence

Table S1. The relative energy of each intermediate states in intra-polymer mechanism. Units in eV. Reaction energies for rate-limiting steps are highlighted in red.

	Gamma point	2×2 *k*-point	3×3 *k*-point
S0	0.00	0.00	0.00
S1	1.37	1.47	1.46
ΔE_1	1.37	1.47	1.46
S2	1.27	1.48	1.46
ΔE_2	-0.10	0.01	0.00
S3	2.62	2.92	2.89
ΔE_3	1.35	1.44	1.42
S4	2.42	2.84	2.80
ΔE_4	-0.20	-0.08	-0.09
S5a	2.53	2.77	2.75
ΔE_{5a}	0.09	-0.07	-0.05
S5b	1.84	1.86	1.86
ΔE_{5b}	-0.69	-0.91	-0.89
S6	1.94	1.97	1.97
ΔE_6	0.10	0.11	0.11
S7	2.97	3.09	3.08
ΔE_7	1.03	1.12	1.11
S8	2.67	2.85	2.87
ΔE_8	-0.30	-0.24	-0.21
S9	4.10	4.47	4.42
ΔE_9	1.43	1.62	1.55
S10	3.44	3.94	3.84
ΔE_{10}	-0.66	-0.53	-0.58
S11	3.91	4.13	4.12
ΔE_{11}	0.47	0.19	0.28
S12	3.67	3.90	3.87
ΔE_{12}	-0.24	-0.23	-0.25

Table S1 lists the relative energies for each intermediate state in the intra-polymer mechanism and corresponding reaction energies for each step ($\Delta E_n = E_n - E_{n-1}$) with different *k*-point sampling. Most reactions are not significantly affected by denser *k*-point mesh. However, the C-C coupling steps (labeled in red) are sensitive to the *k*-point sampling. Therefore, we investigate the reaction pathway for these steps with 2×2 *k*-point sampling.

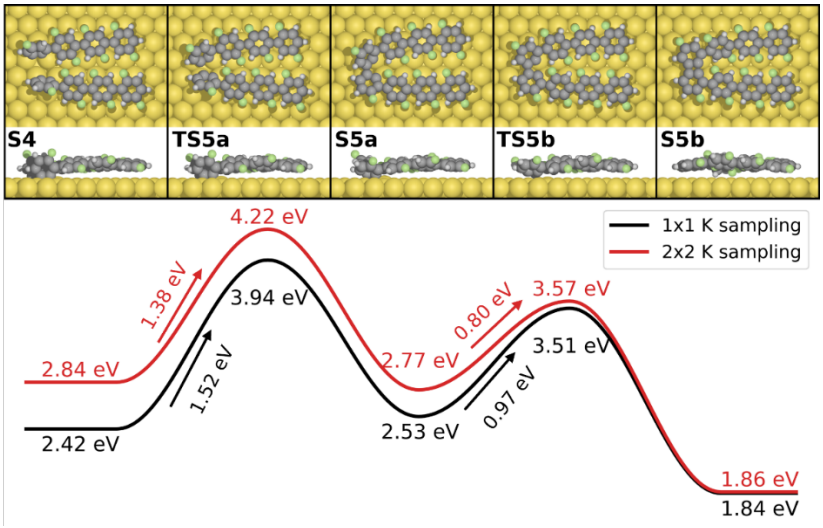

Figure S13. The influence of the *k*-point sampling on the C-C coupling step in the formation of the 1st four-membered carbon ring. Definition of energies are given in **Eq. S3**. The C, H, F, and Au atoms are represented by the gray, white, green, and yellow spheres, respectively.

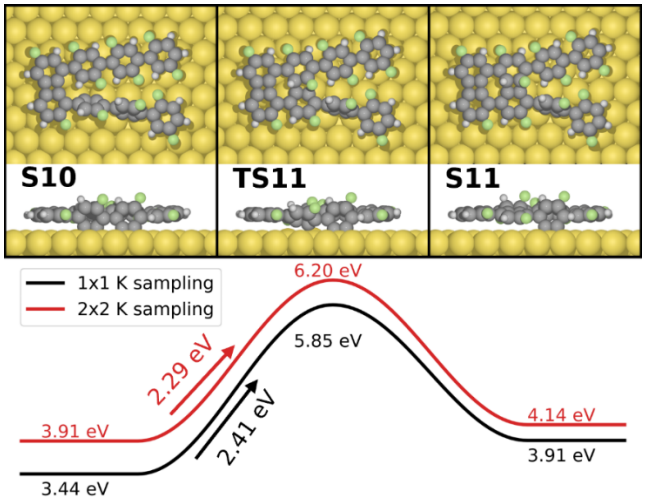

Figure S14. The influence of the *k*-point sampling on the C-C coupling step in the formation of the 2nd four-membered carbon ring. Definition of energies are given in **Eq. S3**. The C, H, F, and Au atoms are represented by the gray, white, green, and yellow spheres, respectively.

As seen in **Figure S13** and **Figure S14**, activation energies for key C-C coupling steps in intra-polymer mechanism decrease with 2×2 *k*-point sampling. Such increased activity indicates that the rate-limiting barriers for the intra-polymer mechanism will converge to around 2.3 eV, agreeing to the high temperature obtained from experiments.[12]

Gibbs free energy calculations

The thermodynamic characteristics for rate-limiting steps are evaluated by the Gibbs free energy profiles, within the Harmonic approximation, in which the Gibbs free energy for each intermediate and transition states are[13]

$$G_{Sx} = H_{Sx}^{elec} + H_{Sx}^{vib}(T) - TS_{Sx}^{vib}(T) \quad \text{(S7)}$$

in which the H_{Sx}^{elec} and H_{Sx}^{vib} are the electronic enthalpy and vibrational enthalpy, respectively. The former can be obtained directly from DFT calculations, while the latter is given as:

$$H_{Sx}^{vib}(T) = k_B \sum_i \left(\frac{h\nu_i}{k_B} + \frac{h\nu_i}{k_B} \frac{1}{e^{h\nu_i/k_BT}-1}\right) \quad \text{(S8)}$$

The vibrational enthalpy is

$$S_{Sx}^{vib}(T) = k_B \sum_i \left(\frac{h\nu_i}{k_BT} \frac{1}{e^{\frac{h\nu_i}{k_BT}}-1} - \ln\left(1 - e^{-h\nu_i/k_BT}\right)\right) \quad \text{(S9)}$$

Herein, *T* is the reaction temperature (selected as 700 K). h and k_B are the Planck's constant and the Boltzmann constant, respectively. ν_i is the vibrational frequency of eigenmode *i*.

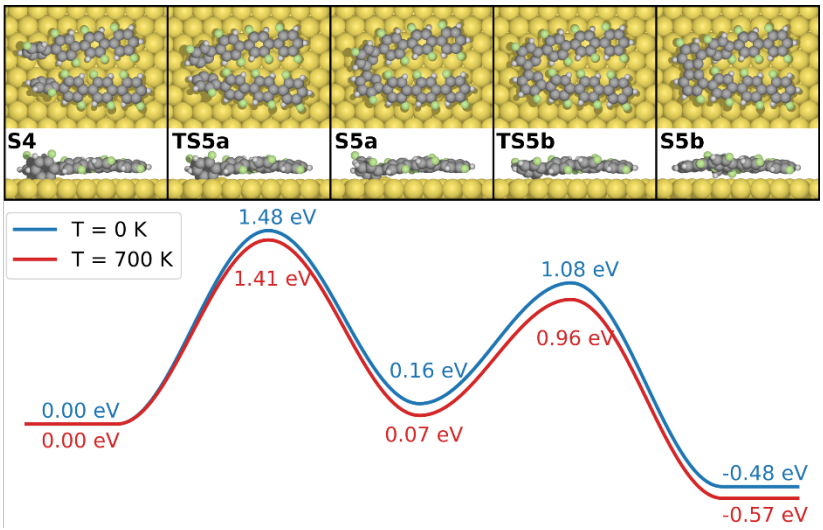

Figure S15. The free energy profiles for the C-C coupling step in the formation of the 1st four-membered carbon ring. The blue and the red curve represent the temperature at 0 K and 700 K, respectively. Corresponding transition states energies only considering electronic enthalpy are 1.52 eV (**TS5a**) and 0.97 eV (**TS5b**). The C, H, F, and Au atoms are represented by the gray, white, green, and yellow spheres, respectively.

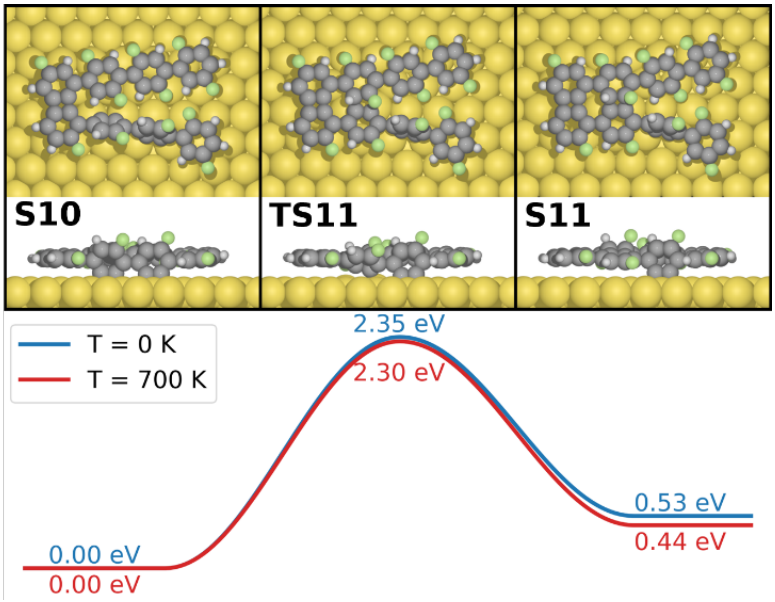

Figure S16. The free energy profiles for the C-C coupling step in the formation of the 2nd four-membered carbon ring. The energy barrier with only electronic enthalpy for **TS11** is 2.41 eV. The blue and the red curve represent the temperature at 0 K and 700 K, respectively. The C, H, F, and Au atoms are represented by the gray, white, green, and yellow spheres, respectively.

At 0 K, there is no contribution from the vibrational entropy to the Gibbs free energy, and the only contribution from the vibrational enthalpy is from the zero-point energy (ZPE). As seen in **Figure S15**-**S16**, the contribution of the ZPE to the energy profile is less than 0.1 eV (comparing the blue curve to the black curve in **Figure S13**-**S14**). In addition, the Gibbs free energy profiles at 700 K exhibit limited change with respect to the potential energy profiles in **Figure 4** and **Figure 7** in the main text, in which the limiting barriers decrease with the order of 0.1 eV. Therefore, the potential energy profiles presented in the main text are sufficient to understand the reaction mechanism.

STM simulations

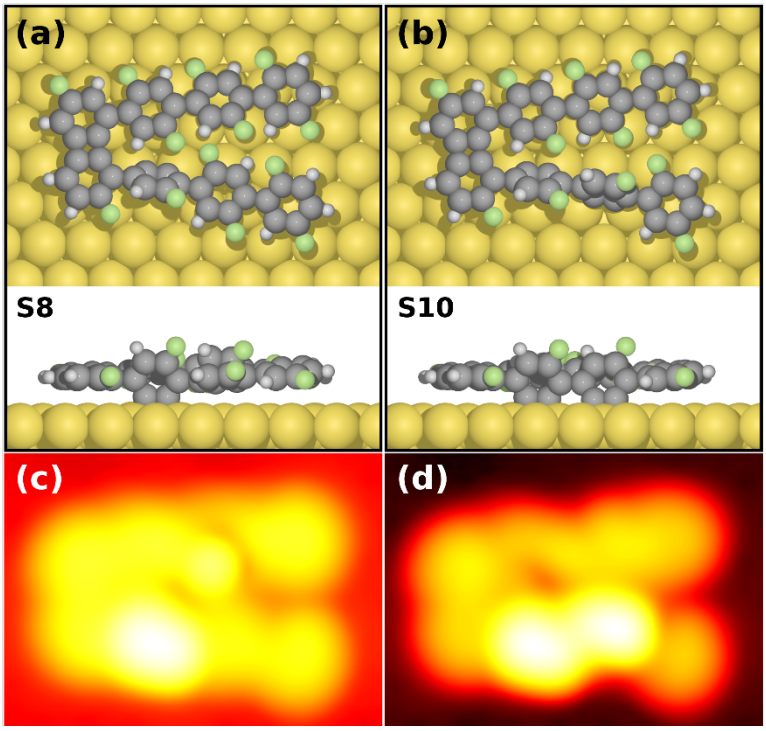

Figure S17. Top and side views of optimized structures for key intermediate state (a) **S8** and (b) **S10** (see **Figure 7** in the manuscript) with standing phenylene groups on the Au(111). (c) and (d) are the simulated STM images for **S8** and **S10**, respectively. The standing phenylene groups appear as the bright protrusions in the simulated images. The STM simulations were obtained as the constant integrated local density of states (LDOS), for energies between the Fermi level (E_F) and $E - E_F = -0.5$ eV, corresponding to a constant current image acquired for a bias of -0.5 V.

References

1 G. Kresse and J. Furthmuller, *Phys. Rev. B* 1996, **54**, 11169–11186.

2 A. Hjorth Larsen, J. Jorgen Mortensen, J. Blomqvist, I. E. Castelli, R. Christensen, M. Dulak, J. Friis, M. N. Groves, B. Hammer, C. Hargus, E. D. Hermes, P. C. Jennings, P. Bjerre Jensen, J. Kermode, J. R. Kitchin, E. Leonhard Kolsbjerg, J. Kubal, K. Kaasbjerg, S. Lysgaard, J. Bergmann Maronsson, T. Maxson, T. Olsen, L. Pastewka, A. Peterson, C. Rostgaard, J. Schiotz, O. Schutt, M. Strange, K. S. Thygesen, T. Vegge, L. Vilhelmsen, M. Walter, Z. Zeng and K. W. Jacobsen, *J. Phys. Condens. Matter.* 2017, **29**, 273002.

3 P. Blöchl, *Phys. Rev. B* 1994, **50**, 17953-17979.

4 I. Hamada, *Phys. Rev. B* 2014, **89**, 121103.

5 M. Dion, H. Rydberg, E. Schroder, D. C. Langreth and B. I. Lundqvist, *Phys. Rev. Lett.*, 2004, **92**, 246401.

6 J. Björk and S. Stafström, *ChemPhysChem*, 2014, **15**, 2851–2858.

7 M. Matena, J. Björk, M. Wahl, T. L. Lee, J. Zegenhagen, L. H. Gade, T. A. Jung, M. Persson and M. Stohr, *Phys. Rev. B*, 2014, **90**, 125408.

8 G. Henkelman, B. P. Uberuaga and H. Jonsson, *J. Chem. Phys.*, 2000, **113**, 9901–9904.

9 G. Henkelman and H. Jonsson, *J. Chem. Phys.*, 1999, **111**, 7010–7022.

10 J. Tersoff and D. R. Hamann, *Phys. Rev. Lett.*, 1983, **50**, 1998–2001.

11 N. Lorente and M. Persson, *Faraday Discuss.*, 2000, **117**, 277–290.

12 Q. Fan, L. Yan, M. W. Tripp, O. Krejčí, S. Dimosthenous, S. R. Kachel, M. Chen, A. S. Foster, U. Koert, P. Liljeroth and J. M. Gottfried, *Science*, 2021, **372**, 852–856.

13 J. Björk, *J. Phys. Chem. C*, 2016, **120**, 21716–21721.

14 M. W. Chase, *J. Phys. Chem. Ref. Data*, 1998, **9**, 1310.